where T_{cs} is the antenna temperature under clear sky conditions, typically 30K and T_{ant} is the radiometer measured antenna temperature. The effective medium temperature T_m has been optimised to 290K. The beacon data represent the attenuation with respect to free space (AFS) which is the sum of attenuation with respect to clear air (ACS) and that due to gaseous absorption (AGS). Scintillations due to atmospheric refractivity are superimposed on the fading due to ACS and AGS. The fade duration from the beacon measurements presented in this Letter represents AFS only. However, it has been found that the gaseous absorption is ~0.115dB and cloud attenuation is ~0.1dB at this frequency. Because of their rapid fluctuations, fade compensation algorithms generally filter out the scintillation effects. In the present analysis we have used a 10s moving average filter to remove the scintillation effects.

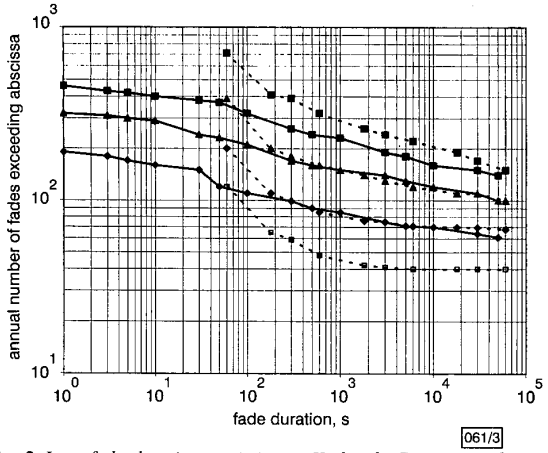

Fig. 3 *Inter-fade duration statistics at Ku-band: Comparison between INTELSAT beacon and radiometer*

—■— RDM (3dB)
—▲— RDM (5dB)
—◆— RDM (10dB)
- -■- - BCN (3dB)
- -▲- - BCN (5dB)
- -◆- - BCN (10dB)
- -□- - BCN (15dB)

Fade duration statistics: The fade duration (FD) is the length of the time in seconds for which the attenuation exceeds a specified threshold level. As a mathematical expression, for a given threshold attenuation A_T if $A \geq A_T$ and $t_1 < t < t_2$, the fade duration is defined as

$$FD_{A_T} = t_2 - t_1 \tag{2}$$

Fig. 1 shows the fade duration statistics obtained with a radiometer (denoted as RDM in Fig. 1) which are compared with those obtained with a beacon (denoted as BCN). Close agreement between the radiometer and beacon measurements can be seen in Fig. 1. The agreement is much better for fade levels of ≥ 5dB. For reference, the 5, 10, 15, 20 and 25dB fades are exceeded for 0.45, 0.2, 0.07, 0.06 and 0.05% of the year, respectively [5]. For a particular VSAT system with 5dB fade margin, there are ~400 rain events lasting 1s or more when the fade level is ≥ 5dB (data from both radiometer and beacon). Approximately 120 events last longer than 5min. If the maximum allowed fade duration is 10min for a VSAT application then there are ~70 rain events when the fade duration is longer than 10min in a year. Therefore 85% of the total rain events last less than 10min. The fade duration is known to be affected by a large number of random time varying multiplicative environmental parameters at least up to 20dB fade depth. Under those circumstances, normalised fade duration statistics would be more appropriate; this will remove the fade duration dependence on the threshold level. When the data are considered as the percentage of fades exceeding a normalised fade duration it has been found that a lognormal fit (with mean = –1.3 and standard deviation = 2) gives the best approximation to the experimental data as given by eqn. 3.

$$P(D_f \geq x) = \frac{1}{2}\mathrm{erfc}\left(\frac{\ln x - \overline{\ln x}}{\sigma\sqrt{2}}\right) = \frac{1}{x\sigma\sqrt{2\pi}}\int_x^\infty \exp\left(-\frac{1}{2}\left(\frac{\ln x - \overline{\ln x}}{\sigma}\right)^2\right) dx \tag{3}$$

where $x = D/\bar{D}$ is the normalised fade duration, $\bar{D}$ is the average fade duration for a particular threshold (shown in Fig. 2), σ is the standard deviation of $\ln(D/\bar{D})$ (= 2 for the measured data), erfc is the complementary error function and $\overline{\ln x}$ (= –1.3 for the measured data) is the mean of $\ln(x)$. The average fade duration ($\bar{D}$) from beacon measurements has been found to be higher than that obtained from the radiometer measurements.

Inter-fade duration: The inter-fade duration or non-fade duration (NFD) is the complement of the fade duration. It is defined as the continuous time over which the attenuation is lower than a given threshold value ($A \leq A_T$):

$$NFD_{A_T} = t_2 - t_1 \tag{4}$$

where $A \leq A_T$, for $t_1 < t < t_2$.

Fig. 3 presents the inter-fade duration statistics obtained by the radiometer (denoted by RDM) as well as the beacon (denoted by BCN). In this case also, the beacon values agree well with those from the radiometer. For a VSAT system (with 10min inter-fade duration allowance) there are ~172 events when the inter-fade duration is < 10min. In other words for about half of the total (320) events the inter-fade duration is < 10min.

Conclusions: We have presented fade duration and inter-fade duration statistics at Ku-band, obtained from an INTELSAT beacon and dual-slope radiometer. The results for both the measurements agree closely with each other. The normalised fade duration follows a lognormal pattern with a mean of –1.3 and standard deviation 2. For VSAT applications with a 5dB fade margin, the average fade duration is ~6min and a 5dB fade depth is exceeded 0.45% of the time in a year. The inter-fade duration for half of the rain events in a year is < 10min.

27 March 2000
Electronics Letters Online No: 20000677
DOI: 10.1049/el:20000677

K.I. Timothy, J.T. Ong and E.B.L. Choo (*School of Electrical and Electronic Engineering, Nanyang Technological University, Singapore 639798, Republic of Singapore*)

E-mail: ekudari@ntu.edu.sg

References

1 FUJITA, M., SHINOZUKA, T., IHARA, T., FURUHAMA, Y., and INUKI, H.: 'ETS-II experiments part IV: Characteristics of millimetre and centimetre wavelength propagation', *IEEE Trans.*, 1980, **AES-16**, pp. 581–589
2 COX, D.C., and ARNOLD, H.: 'Results from the 19- and 28-GHz COMSTAR satellite propagation experiments at Crawford Hill', *Proc. IEEE*, 1982, **70**, pp. 458–488
3 DINTELMANN, F.,: 'Analysis of 11GHz slant path fade duration and fade slope', *Electron. Lett.*, 1981, **17**, (7), pp. 267–268
4 AJAZ, H., and SAFAAI-JAZI, A.: 'Fade and inter-fade duration in Ku and Ka-band frequencies measured from the OLYMPUS satellite beacons'. Virginia Tech, Blacksburg, SATCOM Rep. 93-17, October 1993
5 CHUNNING, Z.: 'Characterisation of rainfall rate and rain attenuation at Ku-band for earth space communication'. M.Eng. Thesis, Nanyang Technological University, Singapore, 1998

Fast ray tracing procedure using space division with uniform rectangular grid

Zhengqing Yun, M.F. Iskander and Zhijun Zhang

A fast ray tracing procedure using space division is presented with the assumption that the reflection/transmission surfaces exactly coincide with the grid lines. Cleary's algorithm is used for the fast space traversing of a ray. The CPU time for the proposed method is approximately 14% of that of the visibility procedure.

Introduction: The ray tracing method can provide site-specific propagation information and is very useful in the development of advanced wireless communication systems, particularly for pico- and micro-cell regions [1]. The conventional ray tracing method is inefficient when the number of involved reflection/transmission objects is large. Many modifications have been proposed to speed up the ray tracing procedure [2, 3], for example, the image method, the utilisation of visibility, and the space division method.

In this Letter we propose an application of the space division method with a uniform rectangular grid to the cases where the walls are located exactly on the grid lines. This situation is common for some office buildings and Manhattan-type outdoor environments. A formulation for 2D cases is presented and the extension to 3D cases is straightforward.

Space division formulation: Consider a layout of the third floor of an office building in Fig. 1. There are 216 rooms and ~310 walls. Using a square grid with cell dimensions of $\Delta_x = \Delta_y = 1.68$m, the floor can be discretised into 65 × 40 cells. Each cell is assigned a label according to the room to which it belongs. Cells in the same room have the same labels, while cells in different rooms are labelled with different numbers. A cell which does not belong to any room (e.g. corridors) is labelled 0. Fig. 2 shows the labelling scheme. Each cell has a unique ID defined by (i, j), with $i = 1, 2, ..., 65$ and $j = 1, 2, ..., 40$. A two-dimensional array, $C(65, 40)$, is created to store the cell labels, i.e. $C(i, j)$ = the label of cell (i, j).

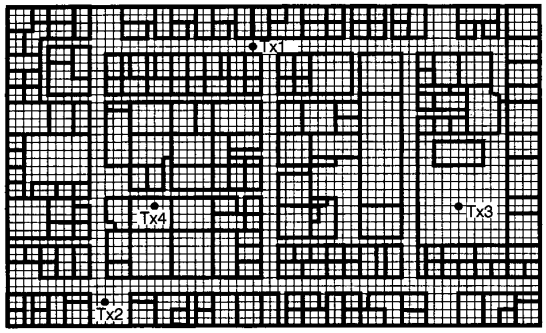

Fig. 1 *Top view of ME Building, 3rd floor*

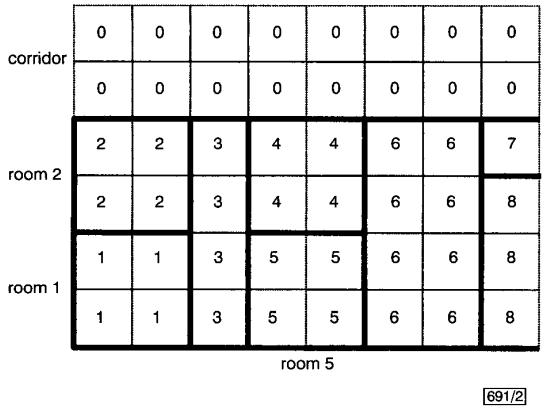

Fig. 2 *Cell labelling scheme*

Algorithm: A ray is defined by a position vector $\mathbf{p}$ and a direction angle θ, denoted by $(\mathbf{p}, \theta)$. Consider a ray $(\mathbf{p}_0, \theta_0)$ as shown in Fig. 3. We first find the ID, denoted by (i_0, j_0), of the cell where the ray is launched. The label of the cell is $C(i_0, j_0)$. Using Cleary and Wyvill's [4] algorithm, the next cell, (i_1, j_1), into which the ray will enter, can be determined efficiently. The new cell label is $C(i_1, j_1)$. If $C(i_0, j_0) = C(i_1, j_1)$ then no wall is hit by the ray while if $C(i_0, j_0) \neq C(i_1, j_1)$ a wall will be intersected by the ray. The intersection point $\mathbf{p}_1$ and the angle θ_1 of the reflected or transmitted ray are calculated. The new ray $(\mathbf{p}_1, \theta_1)$ can be further traced using the same procedure. The procedure continues until the ray is received by the receiving antenna or when some other criteria are met.

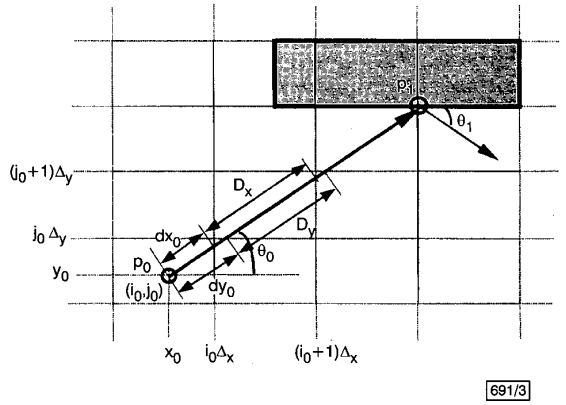

Fig. 3 *Cell traversing of ray*

In the above procedure the algorithm developed by Cleary and Wyvill [4] was employed to find the new cell. The following is a brief description of the algorithm considering the case in Fig. 3. We keep two lengths, dx_0 and dy_0, for a ray. Here dx_0 is the ray length between vertical lines $x = x_0$ and $x = i_0\Delta_x$ while dy_0 is the ray length between horizontal lines $y = y_0$ and $y = j_0\Delta_y$ (see Fig. 3).

If $dy_0 > dx_0$, just as the case in Fig. 3, a vertical grid line will be hit by the ray and the new cell will be the neighbouring cell to the right (or left) side of the current cell with ID $(i_0 + 1, j_0)$ or $(i_0 - 1, j_0)$. If $dy_0 < dx_0$, a horizontal grid line will be hit and the new cell is that for which ID $(i_0, j_0 + 1)$ or $(i_0, j_0 - 1)$. When a vertical or horizontal wall is hit, dx_0 or dy_0 is updated by $dx_0 + D_x$ or $dy_0 + D_y$ where D_x or D_y is the ray length between two neighbouring grid lines $[i\Delta_x, (i + 1)\Delta_x]$ or $[j\Delta_y, (j + 1)\Delta_y]$, respectively. D_x and D_y are constants for a given ray and are easily calculated based on the rectangular dimensions of the grid and the ray angle θ.

Results: To compare the computation time for ray tracing programs, it is reasonable to trace all possible rays without carrying out any receiving detection. In our case we launch 360 rays originating from one source point with different directions. The program traces each ray until the reflection number for the ray exceeds a pre-set limit (40 in the following).

Table 1: CPU time [s] for two ray tracing procedures

Source position	Uniform grid method	Visibility method	Ratio (uniform/visibility)
			%
Tx1	33.68	389.15	8.65
Tx2	40.46	362.19	11.17
Tx3	57.92	275.62	21.01
Tx4	36.69	165.87	22.12
Average	42.19	298.21	14.15

Table 1 shows the CPU time for the two methods. All programs were written using Matlab and run on UltraSPARC-II (296MHz) workstations. Since the CPU time for the visibility method depends on the number of visible surfaces involved in the ray tracing procedure, we selected four locations of sources in the propagation region (see Fig. 1). When source points are located at Tx1 and Tx2, the number of visible surfaces involved is large. The number of visible surfaces is reduced when source points are located at Tx3 and Tx4. Results in Table 1 show that on average the CPU time for the proposed procedure is 14% that of the visibility ray tracing calculations.

Outdoor-to-indoor implementation: If a building can be discretised using the above method, the outdoor-to-indoor propagation can be easily implemented. Detailed results for this application and further integration of the proposed method with a recently

published procedure based on triangular space division for the outdoor regions [5] will be reported soon in a separate publication.

7 March 2000
Electronics Letters Online No: 20000653
DOI: 10.1049/el:20000653

Zhengqing Yun, M.F. Iskander and Zhijun Zhang (*Electrical Engineering Department, University of Utah, UT 84112, USA*)

E-mail: iskander@ee.utah.edu

M.F. Iskander: Corresponding author

References

1 SEICEL, S.Y., and RAPPAPORT, T.S.: 'Site-specific propagation prediction for wireless in-building personal communication system design', *IEEE Trans. Veh. Technol.*, 1994, **43**, (4), pp. 879–891
2 LIANG, G., and BERTONI, H.L.: 'A new approach to 3-D ray tracing for propagation prediction in cities', *IEEE Trans.*, 1998, **AP-46**, (6), pp. 853–863
3 CATERDRA, M.F., PEREZ, J., SAEZ DE ADANA, F., and GUTIERREZ, O.: 'Efficient ray-tracing techniques for three-dimensional analyses of propagation in mobile communications: application to picocell and microcell scenarios', *IEEE Antennas Propagat. Mag.*, 1998, **40**, (2), pp. 15–28
4 CLEARY, J.G., and WYVILL, G.: 'Analysis of an algorithm for fast ray tracing using uniform space subdivision', *Visual Comput.*, 1998, **4**, pp. 65–83
5 ZHANG, Z., YUN, Z., and ISKANDER, M.F.: 'Ray tracing method for propagation models in wireless communication systems', *Electron. Lett.*, 2000, **36**, (5), pp. 464–465

High resolution position estimation using partial pulses

P. Winton and E. Hämmerle

The fundamental principles of radio frequency partial pulses for indoor position location are presented. It is shown experimentally that root-mean-squared x and y position error values of less than 0.1m can be obtained. The advantages of partial pulses over spread spectrum are also noted.

Introduction: Factories of tomorrow need to become increasingly competitive to survive. One area that has been identified as being a possible source of increased productivity is indoor position location. Indoor position location systems could be used to determine the unknown position of products and resources within a production environment, guide vehicles around the factory and locate staff. Current position location methods fail to provide the accuracy and robustness necessary for such applications or are too expensive to be employed in most manufacturing environments. Alternative methods such as spread spectrum systems also have limitations imposed by multiple signal paths (multipath) that have yet to be effectively and efficiently overcome. To overcome the limitations of existing techniques, a new method, referred to here as partial pulse positioning, has been developed. Partial pulse positioning employs a radio frequency (RF) pulse transmitter mounted on items the position of which is to be estimated. The remainder of this Letter outlines the fundamentals of this new method and demonstrates the feasibility by way of experimental results.

Fundamentals of partial pulse positioning: Partial pulse positioning (P^3) is the use of the multipath free section of a received RF pulse, referred to here as the partial pulse. More specifically, the partial pulse is the section of the received signal between the onset time of the line-of-sight (LOS) component and the time of arrival of the first multipath component. This is possible in manufacturing environments as there can always be a RF line-of-sight path between a transmitter and a number of receiving antennas. The received signals are typically bandpass filtered before being digitally sampled in accordance with Nyquist criteria. The multipath-free section of the received signal is extracted by pre-estimating the onset time of the signal at each receiver and, based on the factory geometry, pre-estimating the time of arrival of the first multipath component. It is shown experimentally that this channel pre-estimation is not a major hindrance in determining the position. Traditionally, RF pulse position estimation techniques involve estimating the differential time of arrival (the delays) at a number of spatially separated receivers using cross correlation methods. These delays are proportional to the range differences which constrain the transmitter to lie on a hyperbolic line of position in 2D. Multiple spatially independent RD permit the estimation of position [1]. Owing to channel pre-estimation, the partial pulses cannot be guaranteed to be time shifted replicas of one another and accordingly the cross correlator may give sub-optimal delay estimates.

Delay estimation using partial pulses: To estimate the unknown delay, τ_{dij}, between partial pulses recorded at any two antennas (i and j), the unknown onset times (τ_{0i} and τ_{0j}) and amplitudes (b_i and b_j) at each antenna must be estimated by maximising an *a posteriori* density function $p(\theta_i|\mathbf{y}_i)$ where $\mathbf{y}_i$ is the recorded partial pulse time series and $\theta_i = [\tau_{0i}, b_i]^T$ is the unknown parameter vector (and similarly for antenna j). The difference between the two onset times estimates is the delay estimate. The remainder of the discussion focuses on the estimation of the delay for a partial pulse captured at two antennas. The principles are easily extended to the multiple antenna case. Since the pulse is band-pass filtered, the resulting *a posteriori* density function is cyclic with many adjacent lobes of similar magnitude. If the signal-to-noise ratio (SNR) is high, an appropriate search strategy will determine the arrival time estimate by finding the global maxima of the *a posteriori* density function. However, below a critical SNR the selection of the global maxima will result in onset time and accordingly delay errors that are integer multiples of the carrier period. This phenomenon has been investigated previously for temporally resolvable pulses [2].

These problems can be alleviated by noting that there is a large amount of information available on the probable item location, and therefore the probable delay. The information may take the form of previous position estimates or a more complex probability model. First θ_i is estimated by maximising the *a posteriori* probability density corresponding to the data vector $\mathbf{y}_i$. Typically the time series having the highest SNR will be used to estimate θ_i. It is in the estimation of θ_j that the *a priori* probability density of τ_{dij} becomes invaluable. For the purpose of estimating θ_j it is useful to assume that the conditional density function $p(\mathbf{y}_j|\theta_j)$ is discrete. The discrete components correspond to the maxima of the conditional density function and can be viewed as Dirac delta functions scaled in accordance with the magnitudes of the maxima of the continuous conditional density. This reduces the problem of estimating θ_j to one of maximising a discrete *a posteriori* probability density. The use of a discrete conditional function eliminates any bias that may be introduced through the use of a non-uniform prior density. This technique effectively eliminates the cycle errors that plague delay estimates when the SNR is below threshold.

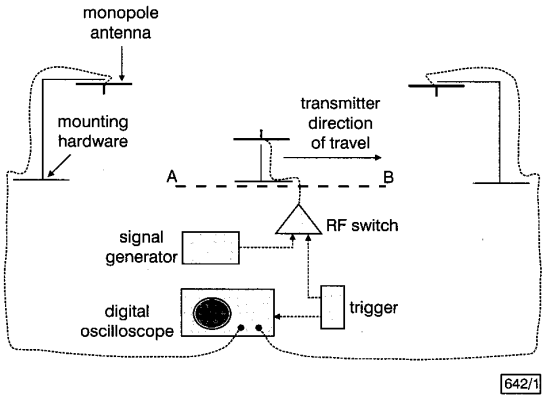

Fig. 1 *Schematic diagram of experimental setup*

Experimental procedure and results: An experimental rig was developed to demonstrate the effectiveness of partial pulse positioning. This rig was used to track the delay as the transmitter was moved along a horizontal path between two receiving antennas in a labo-